A New Method for pHEMT Noise-Parameter Determination Based on 50-Ω Noise Measurement System

Jianjun Gao, Choi Look Law, Hong Wang, Sheel Aditya, and Georg Boeck, *Senior Member, IEEE*

***Abstract*—A new method for determining the four noise parameters of pseudomorphic high electron-mobility transistors (pHEMT) based on 50-Ω noise measurement system without a microwave tuner is presented. The noise parameters are determined based on the noise correlation matrix technique by fitting the measured noise figure of the active device. On-wafer experimental verification up to 26 GHz is presented and a comparison with a tuner-based method is given. The scaling rules for noise parameters have also been determined. Good agreement is obtained between simulated and measured results for 2 $\times$ 20 μm, 2 $\times$ 40 μm, and 2 $\times$ 60 μm gatewidth (number of gate fingers $\times$ unit gatewidth) 0.25-μm double-heterojunction δ-doped pHEMTs.**

***Index Terms*—Correlation noise matrix, noise measurement, noise parameter.**

I. Introduction

THE COMPLETE characterization of the transistor in terms of noise and scattering parameters is necessary for the computer-aided design (CAD) of a low-noise amplifier. The S-parameters are measured by a vector network analyzer (VNA), whereas the noise parameters cannot be measured directly by an instrument. The full noise characterization of a pseudomorphic high electron-mobility transistor (pHEMT) requires the determination of four noise parameters, i.e., minimum noise figure $F_{\min}$, noise resistance R_n, and optimum source reflection coefficient $\Gamma_{\rm opt}$ (magnitude and phase). The determination of the noise parameters is typically performed by analyzing the variation of the measured noise figure as a function of the source impedance. A minimum of four independent measurements is required. However, for increasing accuracy, more than four measurements are performed usually and curve-fitting techniques are used then to determine the noise parameters [1]–[4]. Although this method gives accurate results, it is time consuming and requires expensive automatic broad-band microwave tuners that involves complex calibration procedures.

Some authors proposed improved methods that are using the equivalent transistor noise model to provide additional information to reduce complexity in the measurement procedure [5]–[9]. Other successful techniques are based on match source reflection 50-Ω measurements system (F_{50}) without an automatic tuner [10]–[12]. Tasker *et al.* [10] assume no correlation between noise source and input temperature T_g, which is simply equal to the ambient temperature, only the unknown output temperature T_d must be determined to extract the noise parameters. Alternatively, the correlation coefficient C is assumed to be purely imaginary and related to P, R by the approximate expression $C \approx \sqrt{R/P}$ to determine noise parameters using F_{50} measurements [11]. A complex mathematical method for determining the noise matrix of active devices based on F_{50} measurements by assuming a linear frequency dependency of elements of an intrinsic noise matrix is proposed by Lazaro *et al.* [12], the calibration procedures are very complex and need to determine the intrinsic parameter $C_{\rm gd}$ and the whole parasitic elements.

In this paper, a new method to determine the four noise parameters of pHEMTs based on a 50-Ω measurement system (F_{50}) without an automatic tuner is proposed. In contrast with previous publications [10]–[12], this method has the following advantages.

1) It needs no complex noise deembedding techniques and calibration procedures.
2) No restrictions are imposed on the noise sources and noise matrix elements.
3) Only the determination of pad capacitances C_{pg}, C_{pd}, and C_{pdg}, series inductances L_g, L_d, and L_s, and drain parasitic resistance R_d is needed, not the determination of the other extrinsic and intrinsic elements.
4) The whole parasitic elements are determined by using a pinchoff condition.
5) An improved method for determination of the initial values of the four noise parameters based on [11] is given; the iterative calculation is very fast.

II. Noise-Parameter Extraction Based on 50-Ω Measurement System (F_{50})

A. Equivalent Noise Circuit Model

From the circuit point-of-view, the FET device can be treated as a black box of a noisy two-port. As is well known, the noise

Manuscript received December 9, 2002; revised April 11, 2003.

J. Gao was with the School of Electrical and Electronic Engineering, Nanyang Technological University, Singapore 639798. He is now with the Institute of High-Frequency and Semiconductor System Technologies, Technische Universität Berlin, 10587 Berlin, Germany.

C. L. Law and S. Aditya are with the School of Electrical and Electronic Engineering, Nanyang Technological University, Singapore 639798.

H. Wang is with the Microelectronics Centre, Nanyang Technological University, Singapore 639798.

G. Boeck is with the Institute of High-Frequency and Semiconductor System Technologies, Technische Universität Berlin, 10587 Berlin, Germany.

Digital Object Identifier 10.1109/TMTT.2003.817680

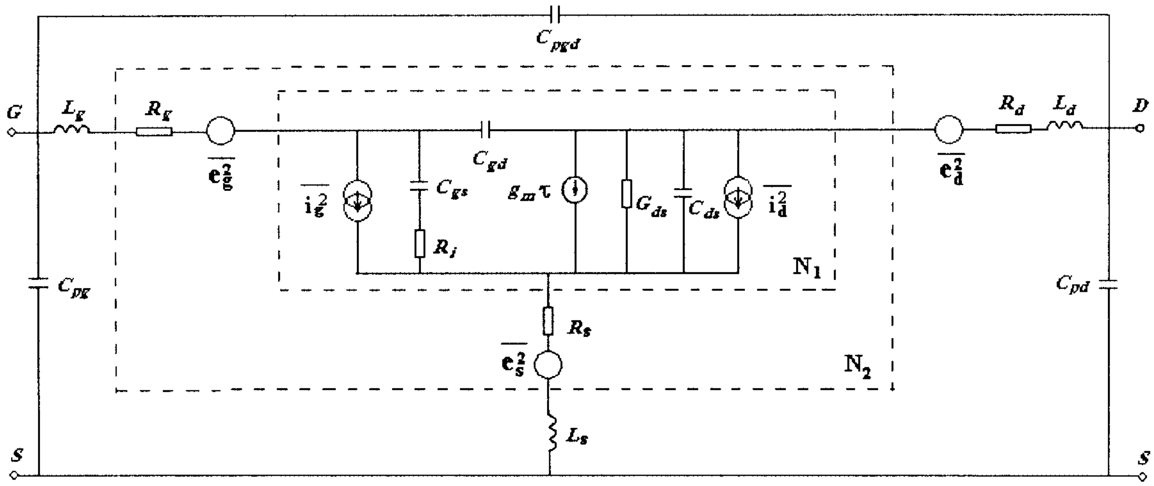

Fig. 1. Noisy small-signal equivalent-circuit model of pHEMT.

behavior of a linear noisy two-port network can be characterized by the four noise parameters $F_{\min}$, R_n, $G_{\rm opt}$, and $B_{\rm opt}$ with

$$F = F_{\min} + \frac{R_n}{G_s}\left[(G_s - G_{\rm opt})^2 + (B_s - B_{\rm opt})^2\right]$$

where F is the noise figure, $Y_s = G_s + jB_s$ is the source admittance, $F_{\min}$ is the minimum noise figure, R_n is the noise resistance, and $Y_{\rm opt} = G_{\rm opt} + jB_{\rm opt}$ is the optimum source admittance.

The equivalent-circuit model of the noisy pHEMT is shown in Fig. 1. The circuit model comprises the well-known small-signal equivalent circuit, and five noise sources $\overline{e_g^2}$, $\overline{e_d^2}$, $\overline{e_s^2}$, $\overline{i_g^2}$, and $\overline{i_d^2}$. The three noise sources $\overline{e_g^2}$, $\overline{e_d^2}$, and $\overline{e_s^2}$ represent the noisy behavior of access resistances R_g, R_d, and R_s and are simply given by $\overline{e_i^2} = 4kTR_i\Delta f$, where k is the Boltzmann constant, T is the absolute temperature, R_i is the resistance value, and Δf is the bandwidth. The two correlated current noise sources $\overline{i_g^2}$ and $\overline{i_d^2}$ represent the internal noise sources of the intrinsic pHEMT.

By neglecting the influence of gate–drain feedback capacitance $C_{\rm gd}$ of the intrinsic equivalent-circuit model of the pHEMT, the calculation of the four parameters can be carried out analytically as follows [13], [14]:

$$F_{\min}^{\rm INT'} = 1 + K_B\omega \tag{1}$$
$$G_{\rm opt}^{\rm INT'} = K_C\omega \tag{2}$$
$$B_{\rm opt}^{\rm INT'} = K_D\omega \tag{3}$$
$$R_n^{\rm INT'} = K_E \tag{4}$$

where $F_{\min}^{\rm INT'}$, $G_{\rm opt}^{\rm INT'}$, $B_{\rm opt}^{\rm INT'}$, and $R_n^{\rm INT'}$ represent intrinsic noise parameters without $C_{\rm gd}$. K_B, K_C, K_D, and K_E are fitting factors, and ω is the angular frequency. From (1)–(4), it can be seen that the equivalent noise resistance $R_n^{\rm INT'}$ is frequency independent, $G_{\rm opt}^{\rm INT'}$ and $B_{\rm opt}^{\rm INT'}$ are proportional to ω, and $F_{\min}^{\rm INT'}$ is a linear function of ω.

B. Influence of $C_{\rm gd}$

However, the gate–drain feedback capacitance $C_{\rm gd}$ is very important because the noise correlation coefficient will be decreased when $C_{\rm gd}$ is neglected. The influence of gate–drain feedback capacitance $C_{\rm gd}$ can be considered using a noise correlation matrix technique.

The Y-parameter noise matrix of the network $N_{\rm GD}$ (not indicated in Fig. 1) only consists of gate–drain feedback capacitance $C_{\rm gd}$. $C_Y^{\rm GD} = 2kT{\rm Re}(Y^{\rm GD})$ is a zero matrix, thus, the intrinsic matrix can be calculated as follows:

$$C_Y^{\rm INT} = C_Y^{\rm GD} + C_Y^{\rm INT'} = C_Y^{\rm INT'} \tag{5}$$

where $C_Y^{\rm INT'}$ is the Y noise matrix of network N_1 (except for $C_{\rm gd}$). $C_Y^{\rm INT'}$ can be determined by translating the chain noise matrix

$$C_{Y11}^{\rm INT'} = C_{A22}^{\rm INT'} + C_{A11}^{\rm INT'}\left|Y_{11}^{\rm INT'}\right|^2 - \left(Y_{11}^{\rm INT'}\right)^* C_{A21}^{\rm INT'} - Y_{11}^{\rm INT'} C_{A12}^{\rm INT'} \tag{6}$$
$$C_{Y12}^{\rm INT'} = C_{A11}^{\rm INT'}\left(Y_{21}^{\rm INT'}\right)^* Y_{11}^{\rm INT'} - C_{A21}^{\rm INT'}\left(Y_{21}^{\rm INT'}\right)^* \tag{7}$$
$$C_{Y21}^{\rm INT'} = C_{A11}^{\rm INT'}\left(Y_{11}^{\rm INT'}\right)^* Y_{21}^{\rm INT'} - C_{A12}^{\rm INT'} Y_{21}^{\rm INT'} \tag{8}$$
$$C_{Y22}^{\rm INT'} = C_{A11}^{\rm INT'}\left|Y_{21}^{\rm INT'}\right|^2 \tag{9}$$

where

$$C_{A11}^{\rm INT'} = R_n^{\rm INT'} \tag{10}$$
$$C_{A22}^{\rm INT'} = R_n^{\rm INT'}\left|Y_{\rm opt}^{\rm INT'}\right|^2 \tag{11}$$
$$C_{A21}^{\rm INT'} = \frac{F_{\min}^{\rm INT'} - 1}{2} - R_n^{\rm INT'}\left(Y_{\rm opt}^{\rm INT'}\right)^* \tag{12}$$
$$C_{A12}^{\rm INT'} = \frac{F_{\min}^{\rm INT'} - 1}{2} - R_n^{\rm INT'} Y_{\rm opt}^{\rm INT'}. \tag{13}$$

The intrinsic chain noise matrix is obtained by translating $C_Y^{\rm INT}$ as follows:

$$C_{A11}^{\rm INT} = \frac{C_{Y22}^{\rm INT'}}{\left|Y_{21}^{\rm INT}\right|^2} \tag{14}$$
$$C_{A21}^{\rm INT} = \frac{Y_{11}^{\rm INT}}{\left|Y_{21}^{\rm INT}\right|^2} C_{Y22}^{\rm INT'} - \frac{C_{Y12}^{\rm INT'}}{\left(Y_{21}^{\rm INT}\right)^*} \tag{15}$$

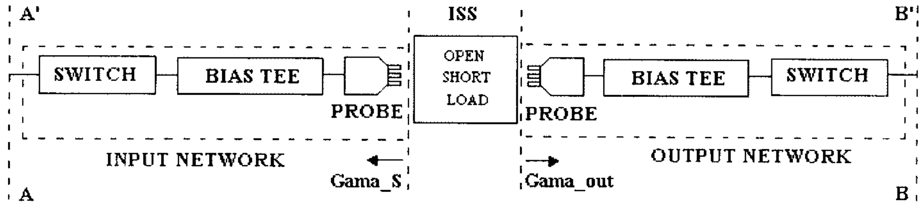

Fig. 2. Block diagram of the input and output network measurement method.

$$C_{A12}^{\rm INT} = \frac{\left(Y_{11}^{\rm INT}\right)^*}{\left|Y_{21}^{\rm INT}\right|^2} C_{Y22}^{\rm INT'} - \frac{C_{Y12}^{\rm INT'}}{Y_{21}^{\rm INT}} \tag{16}$$

$$C_{A22}^{\rm INT} = C_{Y11}^{\rm INT'} + \frac{\left|Y_{11}^{\rm INT}\right|^2}{\left|Y_{21}^{\rm INT}\right|^2} C_{Y22}^{\rm INT'} - \frac{Y_{11}^{\rm INT}}{Y_{21}^{\rm INT}} C_{Y21}^{\rm INT'} - \frac{\left(Y_{11}^{\rm INT}\right)^*}{\left(Y_{21}^{\rm INT}\right)^*} C_{Y12}^{\rm INT'}. \tag{17}$$

Since

$$j\omega C_{\rm gd} \ll Y_{21}^{\rm INT'} \approx g_m \tag{18}$$

we have

$$Y_{21}^{\rm INT} = Y_{21}^{\rm INT'} - j\omega C_{\rm gd} \approx Y_{21}^{\rm INT'} \tag{19}$$

$$Y_{11}^{\rm INT} = Y_{11}^{INT'} + j\omega C_{\rm gd} \propto \omega. \tag{20}$$

The four noise parameters of the intrinsic part are obtained from

$$G_{\rm opt}^{\rm INT} = \sqrt{\frac{C_{A22}^{\rm INT}}{C_{A11}^{\rm INT}} - \left[\frac{{\rm Im}(C_{A12}^{\rm INT})}{C_{A11}^{\rm INT}}\right]^2} = G_{\rm opt}^{\rm INT'} \tag{21}$$

$$B_{\rm opt}^{\rm INT} = \frac{{\rm Im}(C_{A12}^{\rm INT})}{C_{A11}^{\rm INT}} = B_{\rm opt}^{\rm INT'} - \omega C_{\rm gd} \propto \omega \tag{22}$$

$$F_{\rm min}^{\rm INT} = 1 + 2(C_{A12}^{\rm INT} + C_{A11}^{\rm INT} Y_{\rm opt}^{\rm INT}) = F_{\rm min}^{\rm INT'} \tag{23}$$

$$R_n^{\rm INT} = C_{A11}^{\rm INT} = R_n^{\rm INT'} \tag{24}$$

where $F_{\rm min}^{\rm INT}$, $G_{\rm opt}^{\rm INT}$, $B_{\rm opt}^{\rm INT}$, and $R_n^{\rm INT}$ represent intrinsic noise parameters.

From (21)–(24), it is shown that $F_{\rm min}^{\rm INT}$, $G_{\rm opt}^{\rm INT}$, and $R_n^{\rm INT}$ remain invariant and $B_{\rm opt}^{\rm INT}$ remains proportional to ω. Equations (1)–(4) are valid for the intrinsic device where the parasitic resistances due to R_g and R_s only effect the fitting factors. Therefore, the four frequency-dependent noise parameters become four frequency-independent constants. Hence, these can be obtained directly from measurements based on a 50-Ω measurement system.

C. Noise-Parameter-Extraction Procedure

Once the parasitic elements ($C_{pg}, C_{pd}, C_{pdg}, L_g, L_d, L_s, R_d$) are known, the extraction of the four unknown noise parameters can be carried out using the following procedure.

1) Measurement of the S-parameters of the pHEMT.
2) Transformation of the S-parameters to admittance parameters and subtraction of pad capacitances (C_{pg}, C_{pd}, C_{pdg}).
3) Transformation of the Y parameters to impedance parameters and subtraction of the series inductances (L_g, L_d, L_s) and series resistance R_d that correspond to the sub-network N_2.
4) Measurement of the noise figure (F_m) of the system that consists of an input bias network, an output bias network, and the active device.
5) Measurement of the S-parameters of the input and output bias network. The bias networks include coaxial switches, bias tees, probe tips, and cables between them (see Fig. 2) Since the two ports of the bias network are different types, i.e., one port is coaxial and another is coplanar, it is difficult to measure S-parameters using VNA on-wafer measurement directly. Therefore, we use a one-port measurement method to determine the S-parameters of the bias networks.

For a two-port network, the input reflection coefficient can be expressed as a function of the load reflection coefficient

$$S_{\rm in} = S_{11} + \frac{S_{12} S_{21} \Gamma_L}{1 - S_{22}\Gamma_L} \tag{25}$$

where $S_{\rm in}$ is the input and Γ_L is the load reflection coefficient.

First, the one-port coaxial open–short–load (OSL) calibration is performed at plane A-A' (input port measurement) or B-B' (output port measurement); then the S-parameters are measured when the probe tip is connected to the OSL standards on the impedance standard substrate ISS (Cascade Microtech Inc., Beaverton, OR) corresponding to $\Gamma_L = 1, -1$, and 0, respectively. The S-parameters of the bias network can be calculated directly as follows:

$$S_{11} = S_{11}^{\rm LOAD} \tag{26}$$

$$S_{22} = \frac{S_{11}^{\rm OPEN} + S_{11}^{\rm SHORT} - 2S_{11}}{S_{11}^{\rm OPEN} - S_{11}^{\rm SHORT}} \tag{27}$$

$$S_{12} = S_{21} = \sqrt{(S_{11}^{\rm OPEN} - S_{11})(1 - S_{22})} \tag{28}$$

where $S_{11}^{\rm OPEN}$, $S_{11}^{\rm SHORT}$, and $S_{11}^{\rm LOAD}$ are measured input reflection coefficients of the probes if the probe tip is terminated by the OSL standard, respectively.

The source reflection coefficient and the corresponding admittance are shown in Fig. 3. The output reflection coefficient and admittance are shown in Fig. 4. It can be noticed that the system is not an accurate 50-Ω system; the real parts of Y_s and $Y_{\rm out}$ (G_s, $G_{\rm out}$) have small deviations from the 50-Ω system ($G_s = G_{\rm out} = 20$ mS), the imaginary parts of Y_s and $Y_{\rm out}$ (B_s, $B_{\rm out}$) with the small deviations from the 50-Ω system ($B_s = B_{\rm out} = 0$). It can also be observed that Y_s is close to a 50-Ω system as $Y_{\rm out}$

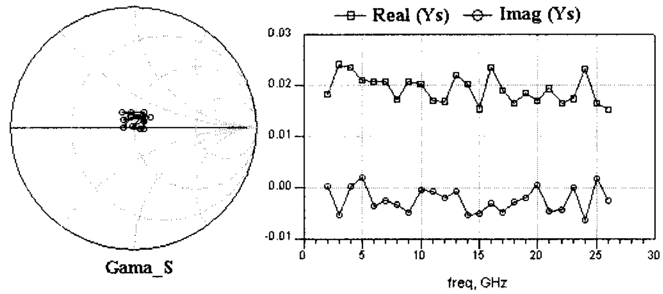

Fig. 3. Source reflection coefficient and admittance.

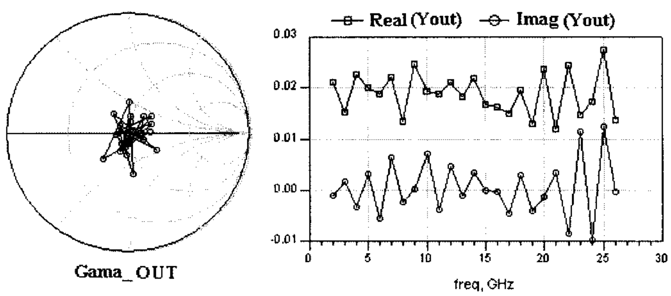

Fig. 4. Output reflection coefficient and admittance.

because a high-performance bias tee has been used at the input. Actually, the perfect 50-Ω system is also not available since the losses of the input and output network cannot be neglected.

The source admittance and the output admittance are

$$Y_s = (20 \pm 5) - j(0 \pm 5) \text{ mS}$$
$$Y_{\text{out}} = (20 \pm 8) - j(0 \pm 11) \text{ mS}.$$

6) Calculate noise figure of device-under-test (DUT).

It is known that the noise figure of a cascade of noisy two ports is given by

$$F_m = F_{\text{IN}} + \frac{F_D - 1}{G_{\text{IN}}} + \frac{F_{\text{OUT}}}{G_{\text{IN}} G_D}. \quad (29)$$

In this case, F_{IN} and G_{IN} are the noise figure and available gain of the input bias network, F_{OUT} is the noise figure of the output bias network, and F_D and G_D are the noise figure and available gain of the DUT.

Since the input and output bias network are passive networks, we get

$$F_{\text{IN}} = \frac{1}{G_{\text{IN}}}$$
$$F_{\text{OUT}} = \frac{1}{G_{\text{OUT}}} \quad (30)$$
$$F_D = G_{\text{IN}} F_m - \frac{1 - G_{\text{OUT}}}{G_{\text{IN}} G_D}. \quad (31)$$

The available gains G_{IN}, G_{OUT}, and G_D are determined by S-parameters, which correspond to the input bias network, output bias network, and active device

$$G_{\text{IN}} = \frac{|S_{21}^{\text{IN}}|^2}{1 - |S_{22}^{\text{IN}}|^2} \quad (32)$$

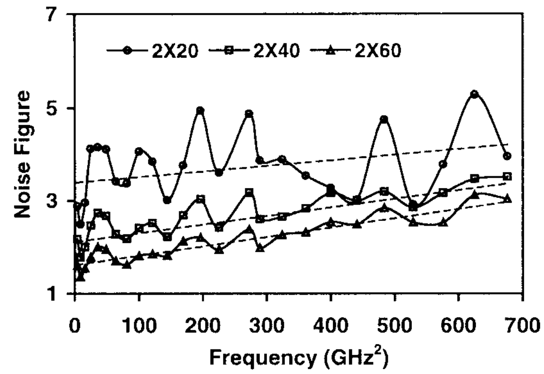

Fig. 5. Evaluation of the noise figures F_{50} of pHEMTs (2×20 μm, 2×40 μm, and 2×60 μm) versus the square of the frequency. Bias condition: $V_{\text{ds}} = 2$ V, $V_{\text{gs}} = 0$ V. ($I_{\text{ds}} = 6, 12, 18$ mA).

TABLE I
INITIAL VALUES OF FOUR NOISE PARAMETERS FOR THREE DIFFERENT SIZE pHEMTs

Device	K_B	K_C	K_D	K_E
2×20um	1.3E-2	5.6E-5	-5.6E-5	120
2×40um	1.0E-2	9.3E-5	-9.3E-5	55
2×60um	8E-3	1.33E-4	-1.33E-4	30

$$G_D = \frac{|S_{21}|^2 (1 - |\Gamma_S|^2)}{|1 - S_{11}\Gamma_S|^2 (1 - |S'_{22}|^2)} \quad (33)$$

where

$$S'_{22} = S_{22} + \frac{S_{12} S_{21} \Gamma_S}{1 - S_{11} \Gamma_{\text{in}}}.$$

The determination of G_{OUT} can be carried out in a similar way as for G_{IN}.

7) Setting initial values of four noise parameters K_B, K_C, K_D, and K_E ($F_{\min}^{\text{INT}}$, $G_{\text{opt}}^{\text{INT}}$, $B_{\text{opt}}^{\text{INT}}$, and R_n^{INT}) and the calculation of the chain noise matrix C_A^D using (1)–(4).

As we know, the accuracy of the numerical optimization methods that minimize the difference between measured and modeled data versus frequency can vary depending upon the optimization method and starting values. Therefore, how to set initial values of K_B, K_C, K_D, and K_E is very important.

A direct extraction method for determining the equivalent noise resistance R_n and the magnitude of the optimum generator admittance $|Y_{\text{opt}}|$ based on a 50-Ω measurement system is proposed by Dambrine *et al.* [11]. Based on this method, an improved method for determining the initial values of all four noise parameters can be used in this paper.

In the case of a 50-Ω generator impedance ($Y_s = G_0 =$ 20 mS), the noise figure can be written as

$$F_{50} = 1 + R_n G_0 + \frac{R_n}{G_0} \left(2 G_0 G_{\text{cor}} + |Y_{\text{opt}}|^2 \right) \quad (34)$$

where G_{cor} is the real part of the correlation admittance. G_{cor} can be approximated by G_{11} (real part of Y_{11}). Since G_{11} is close to zero, G_{cor} can be neglected, and we get

$$F_{50} \approx 1 + R_n G_0 + \frac{R_n}{G_0} |Y_{\text{opt}}|^2. \quad (35)$$

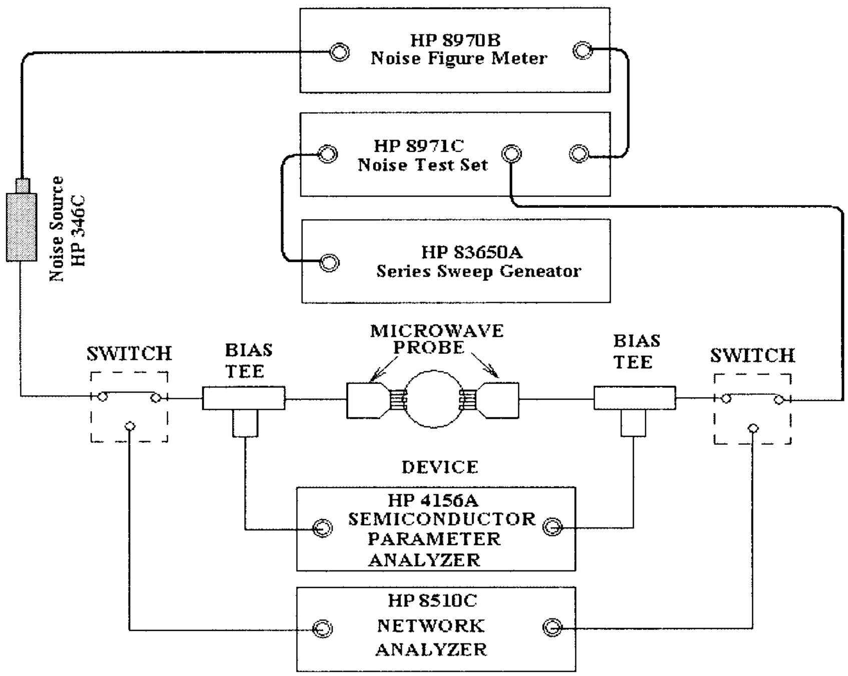

Fig. 6. Microwave transistor S-parameter and noise measurement setup.

Since R_n is nearly frequency independent, while $|Y_{\rm opt}|$ varies proportional to ω^2, the plot of F_{50} versus ω^2 is linear and the value at $\omega = 0$ is $(1 + R_n G_0)$. Thus, R_n can be easily deduced from the F_{50} extrapolation for $\omega = 0$ as follows:

$$R_n \approx \frac{(F_{50}^{\omega=0} - 1)}{G_0}. \tag{36}$$

The slope of F_{50} versus ω^2 provides the magnitude of the optimum generator admittance $|Y_{\rm opt}|$ as follows:

$$|Y_{\rm opt}| \approx \frac{\omega G_0}{2\pi R_n}\sqrt{\text{slope}(F_{50})}. \tag{37}$$

Since the real part $G_{\rm opt}$ and imaginary part $B_{\rm opt}$ have the same order of magnitude, we can set $G_{\rm opt} \approx -B_{\rm opt}$. After R_n and $G_{\rm opt}$ are determined, the initial value of the minimum noise figure $F_{\rm min}$ can be written as

$$F_{\rm min} \approx 1 + 2R_n G_{\rm opt}. \tag{38}$$

The four noise-fitting parameters K_B, K_C, K_D, and K_E are determined using (1)–(4). Fig. 5 shows the experimental evaluations of F_{50} versus the square of the frequency for three different pHEMTs of sizes 2×20 μm, 2×40 μm, and 2×60 μm. The ripple in the graphs is caused by the nonperfect 50-Ω source impedance. It grows up with increasing gatewidth due to deceasing multiplication factor R_n/G_s.

The initial values for the four noise parameters K_B, K_C, K_D, and K_E are summarized in Table I. They have been determined using the above method (the frequency unit is

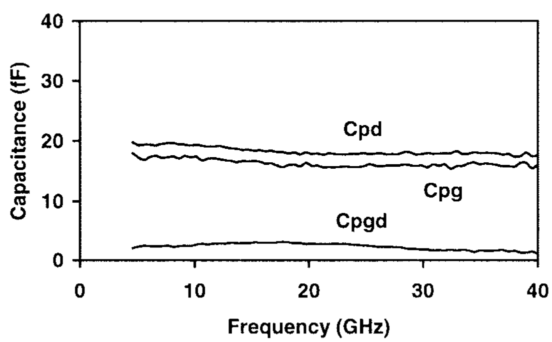

Fig. 7. Extracted pad capacitances.

TABLE II
EXTRACTED PARASITIC INDUCTANCE AND R_d VALUES

Elements	2×20um	2×40um	2×60um
L_g [pH]	95	85	75
L_d [pH]	80	70	60
L_s [pH]	10	10	10
R_d [Ω]	10	5	3.5

gigahertz). The chain noise matrix C_A^D is then determined using (10)–(13).

8) Transformation of the chain noise correlation matrix C_A^D to the impedance noise correlation matrix, and addition of series inductances (L_g, L_d, L_s) and series resistance R_d.
9) Transformation of the impedance noise correlation matrix to the admittance noise correlation matrix, and addition of pad capacitances (C_{pg}, C_{pd}, C_{pdg}).
10) Transformation of the admittance noise correlation matrix to the chain noise correlation matrix, and calculation of the noise figure of the DUT

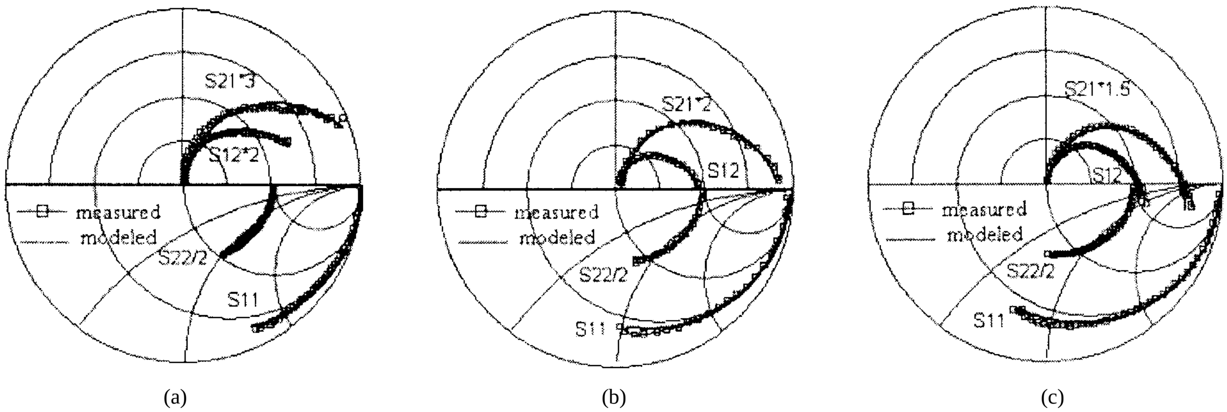

Fig. 8. Comparison of modeled and measured S-parameters for the: (a) 2×20 μm, (b) 2×40 μm, (c) 2×60 μm pinchoff pHEMT. Bias: $V_{\rm gs} = -3$ V, $V_{\rm ds} = 0$ V. The squares indicate the measured values and the lines indicate the modeled ones.

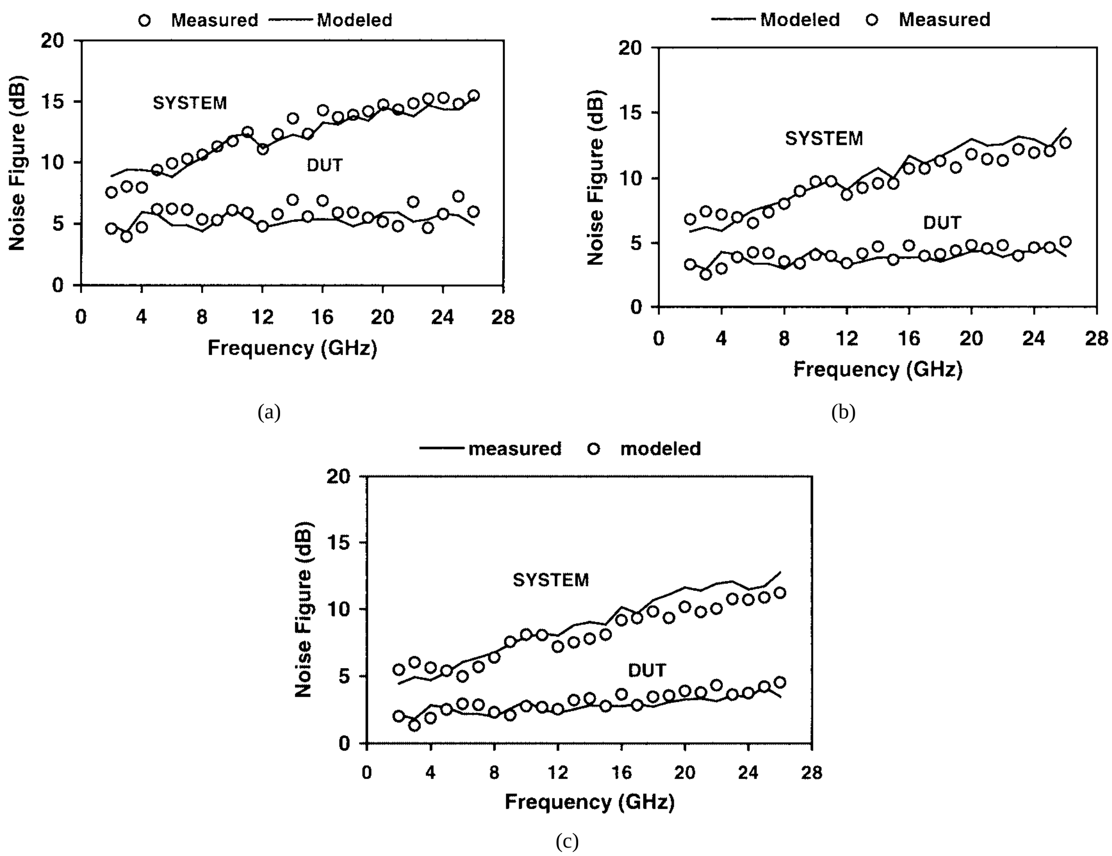

Fig. 9. Comparison of measured and modeled noise figures F_{50} for the: (a) 2×20 μm, (b) 2×40 μm, and (c) 2×60 μm pHEMTs and the system, respectively. Bias condition: $V_{\rm gs} = 0$ V, $V_{\rm ds} = 2$ V ($I_{\rm ds} = 6, 12, 18$ mA).

$$\begin{aligned} F_{\rm MODEL} &= 1 + 2\left[C_{A12} + C_{A11}\left(\sqrt{\frac{C_{A22}}{C_{A11}} - \left[\frac{\mathrm{Im}(C_{A12})}{C_{A11}}\right]^2} \right.\right. \\ &\qquad \left.\left. + j\frac{\mathrm{Im}(C_{A12})}{C_{A11}}\right)\right] \\ &\quad + \left(\frac{C_{A22}}{C_{A11}} + G_S^2 - 2G_S\sqrt{\frac{C_{A22}}{C_{A11}} - \left[\frac{\mathrm{Im}(C_{A12})}{C_{A11}}\right]^2}\right). \end{aligned} \tag{39}$$

11) Calculation of the error criteria as a function of noise figure of the DUT

$$\varepsilon = \frac{1}{N-1}\sum_{i=0}^{N-1} |F_{\rm MODEL}(f_i) - F_{\rm MEASURE}(f_i)|^2 \tag{40}$$

where N is the number of considered frequency points, $F_{\rm MEASURE}(f_i)$ is the measured noise figure at frequency f_i, and $F_{\rm MODEL}(f_i)$ is the calculated corresponding noise figure derived from extracted values of the model parameters.

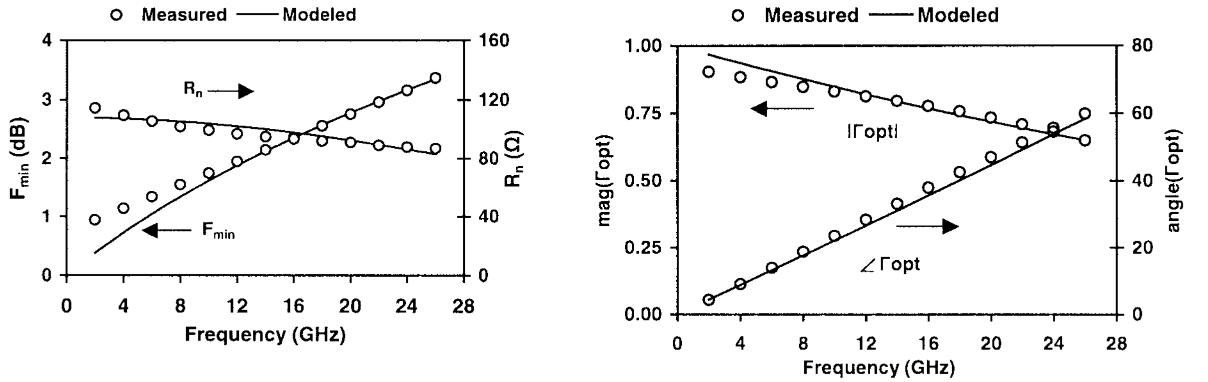

(a) (b)

Fig. 10. Comparison of noise parameters directly measured using a commercial ATN system (o) determined with the new technique (—) for the 2 × 20 μm pHEMT. Bias condition: $V_{\rm gs} = 0$ V, $V_{\rm ds} = 2$ V, $I_{\rm ds} = 6$ mA.

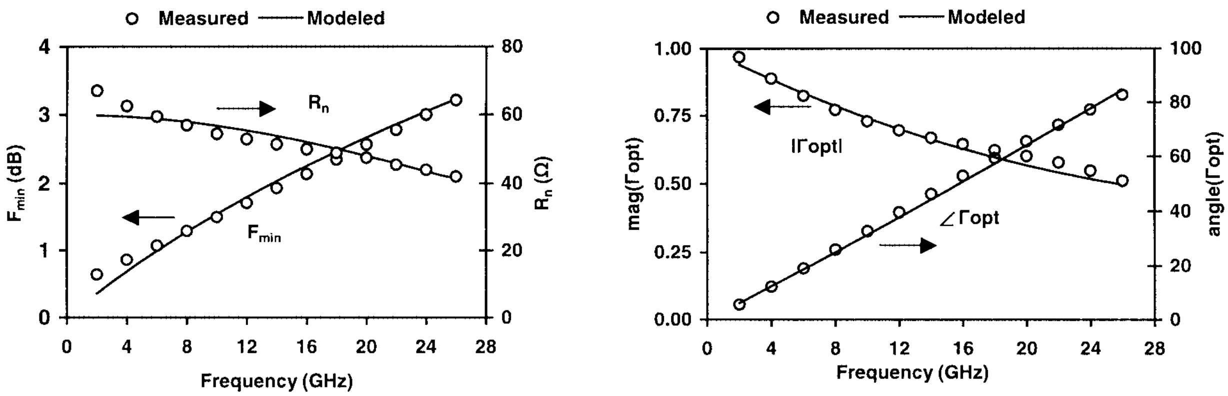

(a) (b)

Fig. 11. Comparison of noise parameters directly measured using a commercial ATN system (o) and determined with the new technique (—) for the 2 × 40 μm pHEMT. Bias condition: $V_{\rm gs} = 0$ V, $V_{\rm ds} = 2$ V, $I_{\rm ds} = 12$ mA.

12) If $\varepsilon > \varepsilon_0$, the values of $F_{\min}^{\rm INT}$, $G_{\rm opt}^{\rm INT}$, $B_{\rm opt}^{\rm INT}$, and $R_n^{\rm INT}$ are updated to reduce ε using the least-squares method.

III. Verification and Experimental Results

Fig. 6 shows the experimental setup. It is composed of a wafer-probe station, an automatic network analyzer (ANA) HP 8510C up to 40 GHz, a noise measurement system (NMS) up to 26.5 GHz, and an electronic broad-band noise source HP 346C up to 50 GHz. The NMS consists of a noise-figure test-set HP 8971C and the noise-figure meter HP 8970B. The local oscillator is an HP 83650B synthesized sweeper up to 50 GHz. HP 8971C consists of a low-noise preamplifier, mixer, and YIG filter. The second stage (HP 8970B) is centered at the intermediate frequency IF $= 450$ MHz. DC bias was supplied by an Agilent 4156 A. All measurements were carried out on-wafer using Cascade Microtech Inc.'s Air-Coplanar Probes ACP50-GSG-100. The wafer probes were calibrated using a line-reflect-match (LRM) calibration method for S-parameter measurement.

The noise-parameter measurement method proposed in this paper has been tested on-wafer up to 26 GHz using AlGaAs–InGaAs–GaAs pHEMTs with 0.25-μm mushroom gates, grown and fabricated using Nanyang Technological University's (NTU's), Singapore, in-house developed process technology. The layer structure of the wafer, from bottom to top, consists of a GaAs undoped buffer layer, 140-Å undoped $\rm In_{0.22}Ga_{0.78}As$ strained layer, 40-Å $\rm Al_{0.25}Ga_{0.75}As$ spacer layer, 5×10^{12} cm^{-2} Si δ-doped plane, 220-Å i-$\rm Al_{0.25}Ga_{0.75}As$ source layer, and an Si-doped 450-Å $\rm n^+$–GaAs cap layer.

In this paper, PI-gate pHEMTs with 2×20 μm, 2×40 μm, and 2×60 μm gatewidth (number of gate fingers $\times$ unit gatewidth) and a pinchoff voltage of approximately -0.8 V have been used. In this section, experimental results are presented, and a comparison of the novel method with the tuner-based method is given.

A. Extraction of Parasitic Elements

The three capacitance elements C_{pg}, C_{pd}, and C_{pdg} describe the capacitive effects of the measurement probe contacts. Since the pad profile for all four types of devices is the same, the pad capacitances are determined by measuring an open structure consisting of only the pads. The pad capacitance values are $C_{pg} = 16$ fF and $C_{pd} = 18$ fF. The isolation between the pads is 35 dB, which corresponds to a capacitance C_{pdg} of 2.5 fF. Fig. 7 shows the extracted results of the pad capacitances. Rather constant values are observed over a wide frequency range (4.0$\sim$40 GHz).

In order to extract extrinsic parameters, the conventional cold-FET method applies a strong forward bias to the gate of the FET. However, in the case of a pHEMT, this method may

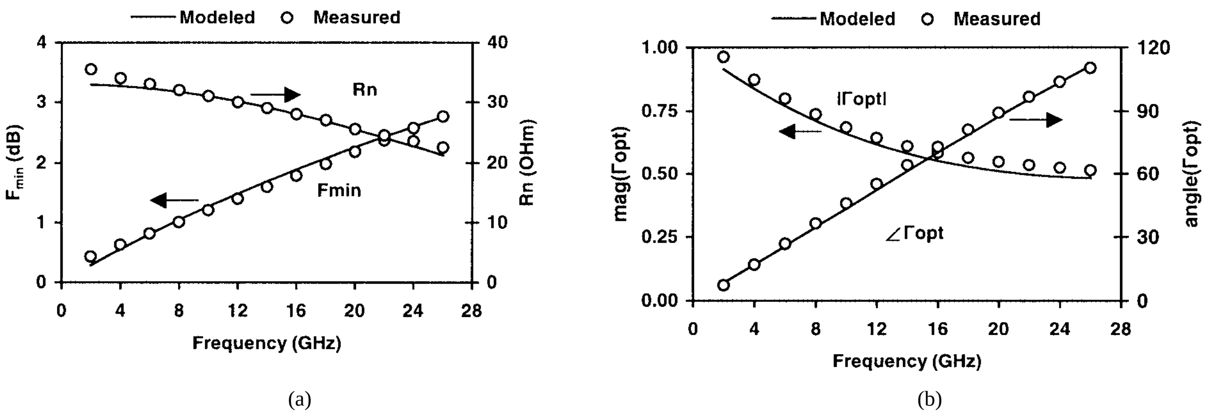

Fig. 12. Comparison of noise parameters directly measured using a commercial ATN system (o) and determined with the new technique (—) for the 2 × 60 μm pHEMT. Bias condition: $V_{\rm gs} = 0$ V, $V_{\rm ds} = 2$ V, $I_{\rm ds} = 18$ mA.

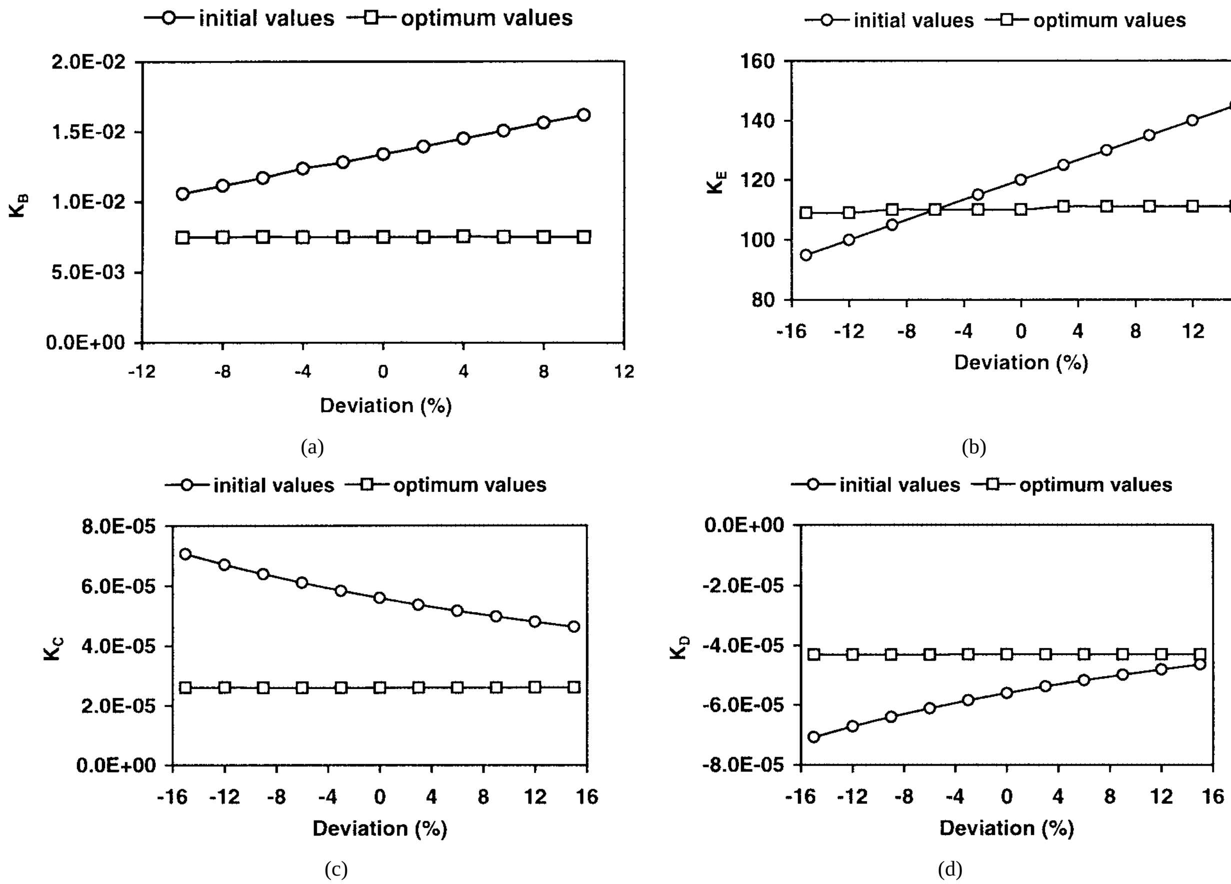

Fig. 13. Noise parameters versus percentage deviation of the straight line for the 2 × 20 μm pHEMT. The initial guess for the straight line is obtained by a simple linear regression applied to the measured noise figures (see Fig. 5).

TABLE III
OPTIMUM VALUES OF NOISE PARAMETERS FOR THREE DIFFERENT SIZE pHEMTs

Elements	K_B	K_C	K_D	K_E
2×20um	7.5E-3	2.6E-5	-4.3E-5	110
2×40um	6.8E-3	4.8E-4	-7.0E-5	60
2×60um	5.4E-2	7.0E-4	-1.0E-4	33

TABLE IV
OPTIMUM VALUES OF NOISE FITTING PARAMETERS FOR THREE DIFFERENT SIZE pHEMTs AFTER MODEL EXTENSION

Elements	K_A	K_B	K_C	K_D	K_E
2×20um	1.14	6.5E-3	2.6E-5	-4.3E-5	110
2×40um	1.05	6.3E-3	4.8E-4	-7.0E-5	60
2×60um	1.0	5.4E-2	7.0E-4	-1.0E-4	33

cause gate degradation due to the large gate current running through the Schottky junction. In this paper, the whole parasitic parameters are extracted by using the pinchoff bias condition only. The dc-bias condition is $V_{\rm gs} = -3$ V, $V_{\rm ds} = 0$ V.

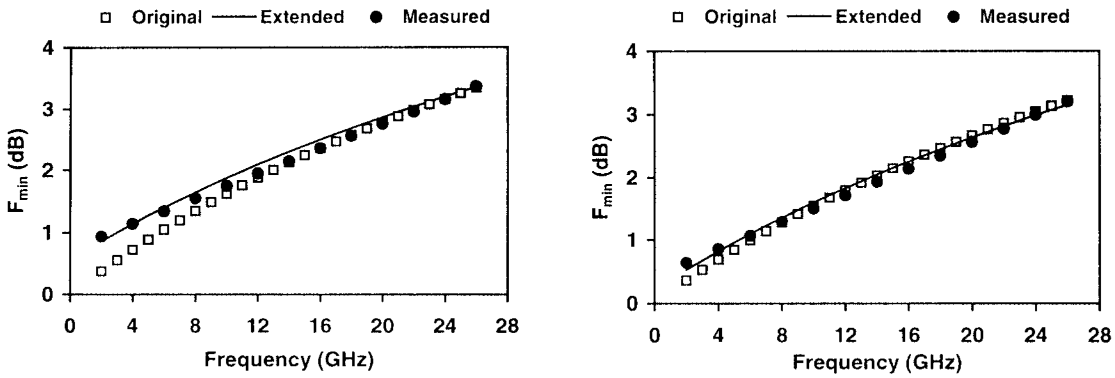

(a) (b)

Fig. 14. Optimum noise figure versus frequency. Comparison of original model, extended model, and measurements for the: (a) 2×20 μm and (b) 2×40 μm devices. Bias condition: $V_{\rm gs} = 0$ V, $V_{\rm ds} = 2$ V ($I_{\rm ds} = 6, 12$ mA).

The three inductances L_g, L_d, and L_s are dependent on the length of the device feed lines and are not scalable. However, the drain resistance R_d is inversely proportional to the size of the device. Table II shows the extracted results of the four parasitic elements.

Fig. 8 compares the measured and modeled S-parameters for the 2×20 μm, 2×40 μm, 2×60 μm, and 2×100 μm pHEMT in the frequency range of 50 MHz–40 GHz. The modeled S-parameters agree very well with the measured ones.

B. Extraction of Noise Parameters

When parasitic elements, pad capacitances, series inductances, and drain resistance are determined, the noise parameters can be obtained by using above method.

Fig. 9(a)–(c) compares the measured and modeled noise figure F_{50} for the 2×20 μm, 2×40 μm, and 2×60 μm, respectively, pHEMT in the frequency range of 2–26 GHz under the bias condition $V_{\rm gs} = 0$ V, $V_{\rm ds} = 2$ V ($I_{\rm ds} = 6, 12, 18$ mA). An adequate comparison for the noise figure of the system is also given in Fig. 10. The modeled noise figures agree well with the measured ones based on the 50-Ω measurement system.

The transistor noise parameters determined from F_{50} by using the new method are compared to the noise parameters measured with the commercial ATN system NP5 based on a broad-band tuner. Figs. 10–12 show these comparisons as a function of frequency. A good agreement between measured and modeled results can be indicated and the validity of the method is confirmed.

A sensitivity study of the extraction method has been performed for the 2×20 μm pHEMT because of the larger ripple. Fig. 13(a)–(d) shows the extracted noise parameters for the 2×20 μm device depending on the percentage deviation of the straight line from the nominal values obtained by a simple linear regression applied to the measured curve. From these diagrams, it can be taken that the final values of the noise parameters show nearly no sensitivity with respect to changes of the initial straight line, whereas, of course, the initial guesses of the noise parameters change.

Table III summarizes the extracted optimum four fitting parameters that correspond to transistor noise parameters. A comparison with Table I proves that initial values and optimum values match very well for noise resistance $K_E(R_n)$. The dispersions between the initial values of K_B, K_C, and K_D ($F_{\min}$, $G_{\rm opt}$, and $B_{\rm opt}$) and optimum values of the large-size devices (2×40 μm and 2×60 μm) are smaller for the small-size devices. The reasons are as follows.

- The system is not an accurate 50-Ω system for the DUT.
- The large-size device satisfies the assumption ($G_{\rm opt} \gg G_{\rm cor}$) better.

After careful examination of the measured data, the scaling formula are determined to be

$$\frac{K_C^{\rm I}}{K_C^{\sqcap}} = \frac{W_g^{\rm I}}{W_g^{\sqcap}} \tag{41}$$

$$\frac{K_D^{\rm I}}{K_D^{\sqcap}} = \frac{W_g^{\rm I}}{W_g^{\sqcap}} \tag{42}$$

$$\frac{K_E^{\rm I}}{K_E^{\sqcap}} = \frac{W_g^{\rm I}}{W_g^{\sqcap}} \tag{43}$$

i.e.,

$$R_n \propto \frac{I}{W} \tag{44}$$

$$G_{\rm opt} \propto W \tag{45}$$

$$B_{\rm opt} \propto W. \tag{46}$$

It is noticed that K_B is not scalable, which means $F_{\min}$ is not dependent on the width. In Figs. 10(a), 11(a), and 12(a), we can find that the modeled optimum noise figure $F_{\min}$ agrees well with the measured $F_{\min}$, especially at high frequencies. However, there are small differences between measured and modeled data at low frequencies; the differences increase if gatewidth decreases. The reason for that lies in a gate leakage current.

It is well established that a short gate on a thin heavily doped layer is necessary to obtain an excellent microwave performance. As a result, problems with gate leakage current and additional noise become significant. Some noise models that take into account the influence of gate leakage current have been reported [15], [16]. For our device, the leakage currents are in the same order for all devices (roughly 1 μA) independent on the gatewidth. This means that the influence of the gate current on noise behavior is larger for small devices than for large ones. Since the extracted noise parameters of our 50-Ω method are based primarily on S-parameters and a model with two noise sources, influence of a gate current is not taken into account in contrast to a complete noise-parameter characterization. However, the influence of a gate current can be considered by introducing a new empirical formula as follows:

$$F_{\min}^{\text{INT}} = K_A + K_B \omega. \quad (47)$$

The extracted optimum five fitting parameters after model extension are summarized in Table IV. We can find that the parameters have small changes for the 2×20 μm and 2×40 μm device, while the parameters remain unvaried for the 2×60 μm device. Fig. 14 shows that the application of the proposed formula leads to a good agreement between modeled and measured optimum noise figures in the entire frequency range for both the 2×20 μm and 2×40 μm devices.

IV. Conclusion

A new method for the determination of noise parameters of pHEMTs based on a 50-Ω NMS without microwave tuners has been proposed, and successfully applied to three devices with different sizes. Good agreement is obtained between simulated and measured results for 2×20 μm, 2×40 μm, and 2×60 μm gatewidths (number of gate fingers $\times$ unit gatewidth) double-heterostructure (DH) pHEMT devices. Noise parameters up to 26 GHz and scaling rules for noise parameters have been determined. A new empirical formula for an optimum noise figure is given, and significant improvement in the accuracy of the optimum noise figure is obtained by using the new expression.

References

[1] R. Q. Lane, "The determining of device noise device," *Proc. IEEE*, vol. 57, pp. 1461–1462, 1969.

[2] G. Caruso and M. Sannino, "Computer-aided determination of microwave two-port noise parameters," *IEEE Trans. Microwave Theory Tech.*, vol. MTT-26, pp. 639–642, Sept. 1978.

[3] A. C. Davidson, B. W. Leake, and E. Strid, "Accuracy improvements in microwave noise-parameter measurements," *IEEE Trans. Microwave Theory Tech.*, vol. 37, pp. 1973–1978, Dec. 1989.

[4] J. M. O'Callaghan and J. P. Mondal, "A vector approach for noise parameter fitting and selection of source admittance," *IEEE Trans. Microwave Theory Tech.*, vol. 37, pp. 1376–1382, Aug. 1989.

[5] M. S. Gupta and P. T. Greiling, "Microwave noise characterization of GaAs MESFET's: Determination of extrinsic noise parameters," *IEEE Trans. Microwave Theory Tech.*, vol. 36, pp. 745–751, Apr. 1988.

[6] M. Pospieszalski, "Modeling of noise parameters of MESFET's and MODFET's and their frequency and temperature dependence," *IEEE Trans. Microwave Theory Tech.*, vol. 37, pp. 1340–1350, Sept. 1989.

[7] R. A. Pucel, "A general noise de-embedding procedure for packaged two-port linear active devices," *IEEE Trans. Microwave Theory Tech.*, vol. 40, pp. 2013–2020, Nov. 1992.

[8] A. Gasmi, B. Huyart, E. Bergeault, and L. P. Jallet, "A new calculation approach of transistor noise parameters as a function of gatewidth and bias current," *IEEE Trans. Microwave Theory Tech*, vol. 45, pp. 338–344, Mar. 1997.

[9] L. Klapproth, A. Schaefer, and G. Boeck, "A bias dependent HEMT noise model," in *IEEE MTT-S Int. Microwave Symp. Dig.*, 1997, pp. 881–884.

[10] P. J. Tasker, W. Reinert, B. Hughes, J. Braunstein, and M. Schlechtweg, "Direct extraction of all four transistor noise parameters using a 50-Ω measurement system," in *IEEE MTT-S Int. Microwave Symp. Dig.*, 1993, pp. 1251–1254.

[11] G. Dambrine, H. Happy, F. Danneville, and A. Cappy, "A new method for on wafer noise measurement," *IEEE Trans. Microwave Theory Tech.*, vol. 41, pp. 375–381, Mar. 1993.

[12] A. Lazaro, L. Pradell, and J. M. O' Callaghan, "FET noise-parameter determination using a novel technique based on a 50-Ω noise-figure measurements," *IEEE Trans. Microwave Theory Tech.*, vol. 47, pp. 315–324, Mar. 1999.

[13] H. Fukui, "Design of microwave GaAs MESFET's for broad band low noise amplifier," *IEEE Trans. Microwave Theory Tech.*, vol. MTT-27, pp. 643–650, July 1979.

[14] A. Cappy, "Noise modeling and measurement techniques," *IEEE Trans. Microwave Theory Tech.*, vol. 36, pp. 1–10, Jan. 1988.

[15] D.-S. Shin, J. B. Lee, H. S. Min, J.-E. Oh, Y.-J. Park, W. Jung, and D. S. Ma, "Analytical noise model with the influence of shot noise induced by the gate leakage current for submicrometer gate-length high-electron-mobility transistors," *IEEE Trans. Electron Devices*, vol. 44, pp. 1883–1887, Nov. 1997.

[16] R. Reuter, M. Agethen, U. Auer, S. van Waasen, D. Peters, W. Brockerhoff, and F.-J. Tegude, "Investigation and modeling of impact ionization with regard to RF and noise behavior of HFET," *IEEE Trans. Microwave Theory Tech.*, vol. 45, pp. 977–983, June 1997.

Jianjun Gao was born in Hebei Province, China, in 1968. He received the B.Eng. and Ph.D. degrees from the Tsinghua University, Beijing, China, in 1991 and 1999, respectively, and M.Eng. Degree from the Hebei Semiconductor Research Institute, Hebei, China, in 1994.

From 1999 to 2001, he was a Post-Doctoral Research Fellow with the Microelectronics Research and Development Center, Chinese Academy of Sciences, where he developed pHEMT optical modulator drivers. In 2001, he joined the School of Electrical and Electronic Engineering, Nanyang Technological University (NTU), Singapore, as a Research Fellow, where he was involved with semiconductor device modeling and on-wafer measurement. Since 2003, he has been a Research Associate with the Institute for High-Frequency and Semiconductor System Technologies, Technische Universität Berlin, Berlin, Germany, where he is involved with InP heterojunction bipolar transistor (HBT) modeling and circuit design for high-speed optical communication.

Choi Look Law received the B.Eng. and Ph.D. degrees from King's College, London, U.K., in 1983 and 1987, respectively.

He is currently an Associate Professor with the School of Electrical and Electronic Engineering, Nanyang Technological University, Singapore. He is also the Director of the Positioning and Wireless Technology Centre, Nanyang Technological University. His research interests are in ultra-wide-band microwave circuit characterization, design and modeling, wide-band channel characterization and effects on high-speed wireless communication, RF identification, wireless networking, and positioning systems. He is a co-founder of RFNET, a company that specializes in RF and wireless working products and services. He has authored or coauthored over 100 conference and journal papers.

Hong Wang received the B.Eng. degree from Zhejiang University, Hangzhou, China, in 1988, and the M. Eng. and Ph.D. degrees from the Nanyang Technological University (NTU), Singapore, in 1998 and 2001, respectively.

From 1988 to 1994, he was with the Institute of Semiconductors, Chinese Academy of Sciences, where he developed InP-based opto-electronic integrated circuits (OEICs). From 1994 to 1995, he was a Royal Research Fellow with British Telecommunications Laboratories, Ipswich, U.K., where he was involved with the development of InP-based HFETs. Since 1996, he has been with the Microelectronics Centre, Nanyang Technological University, where he is currently an Assistant Professor. His current research interests are InP- and GaAs-based compound semiconductor device physics, fabrication technology, and characterization. He has authored or coauthored over 70 technical papers related to his research.

Sheel Aditya received the B.Tech. and Ph.D. degrees in electrical engineering from the Indian Institute of Technology (IIT) Delhi, Delhi, India, in 1974 and 1979, respectively.

From 1979 to 2000, he was a faculty member with the Electrical Engineering Department, IIT Delhi. The last position he held there was that of Professor. He is currently an Associate Professor with the School of Electrical and Electronic Engineering Nanyang Technological University, Singapore. He has held visiting assignments with the Chalmers University of Technology, Göteborg, Sweden, the Indian Institute of Science, Bangalore, India, Florida State University, Tallahassee, and the Nanyang Technological University, Singapore. His teaching and research interests are microwave integrated circuits, quasi-optics, integrated optics, optical-fiber communication, and numerical techniques. He has been involved in a number of research and development projects.

Georg Boeck (M'93–SM'00) was born in Wertingen, Germany, in 1951. He received the Dipl.-Ing. degree in electrical engineering and the doctoral degree from the Technische Universität Berlin, Berlin, Germany, in 1977 and 1984, respectively.

In 1984, he joined Siemens Research Laboratories, Munich, Germany, where his research concerned fiber optics and GaAs electronics. From 1988 to 1991, he was a Full Professor of electronic devices and circuits with the Fachhochschule Regensburg, Regensburg, Germany. Since 1991, he has been a Full Professor of microwave engineering with the Technische Universität Berlin, Berlin, Germany. His main areas of research are characterization, modeling, and design of microwave semiconductor devices, and monolithic integrated circuits [RF integrated circuits (RFICs), monolithic microwave integrated circuits (MMICs)] up to the millimeter-wave range.